Structure of a Midtropospheric Vortex Induced by a Mesoscale Convective System

DIANA L. BARTELS

NOAA/ERL/NSSL/Mesoscale Research and Application Division, Boulder, Colorado

JOHN M. BROWN AND EDWARD I. TOLLERUD

NOAA/ERL/FSL/Forecast Research Division, Boulder, Colorado

(Manuscript received 21 December 1995, in final form 17 May 1996)

ABSTRACT

On 9 June 1988 a mesoscale (~200-km diameter) convectively generated vortex (MCV) passed through the Colorado wind-profiling network. The generating convective system, which was too small to meet Maddox's mesoscale convective complex criteria, developed beneath a high-amplitude mid- and upper-level ridge axis. Profiler winds obtained within the stratiform region of the convective system and near the center of the ensuing MCV form the basis of this study. With the addition of satellite (including rapid scan) images and conventional and Doppler radar data, this vortex was well observed over its entire life cycle.

The slowly moving vortex was observed by the Flagler 50-MHz profiler for more than 16 h. For a portion of this period the circulation was quasi-steady; hence, the spatial structure of the vortex was depicted by time-to-space conversion of the profiler data. The results show a strong, coherent circulation with maximum tangential speeds greater than 16 m s^{-1} at 6 km above mean sea level (MSL) and at radii of 50–70 km; corresponding relative vorticity was more than three times as large as the local Coriolis parameter.

The long duration and the apparent dominance of vorticity over divergence suggest that the flow in the vortex was in a quasi-balanced state. Hence, the temperature perturbation necessary to support the tangential velocity distribution was computed assuming gradient balance in the radial direction. The resulting estimated temperature structure showed a warm core with a magnitude of 2.3°C at 7.3 km MSL and a cold core below 6.3 km MSL. The associated potential vorticity (PV) structure at the vortex center consisted of a lens of high PV with a maximum at 6.3 km MSL and relative minima above and below this height.

1. Introduction

During the next few years operational meteorologists in the United States will continue to be inundated with new observations from both wind profilers and Doppler radars. These data have already revealed many mesoscale phenomena in unprecedented detail. The intent of this paper is to document profiler observations of one such phenomenon, the mesoscale convectively generated vortex (MCV). These residual circulations, hypothesized to be in a state of approximate balance (cf. Davis and Weisman 1994),[1] are generated in at least some mesoscale convective systems (MCSs).

Visible satellite data (e.g., Fig. 1) have previously composed the only routinely available data source capable of observing these mesoscale circulations because their small size (roughly 200–300 km in diameter) renders them only occasionally observable by the conventional sounding network. Because of this, there are only a few documented MCVs each year (Bartels and Maddox 1991). The National Oceanic and Atmospheric Administration Profiler Demonstration Network provides an opportunity to obtain more frequent quantitative observations of MCVs, principally because profilers operate continuously. The network of profilers is also more dense than the sounding network over the central United States, where most MCVs occur.

The first evidence of residual cyclonic circulations associated with midlatitude systems was provided by Johnston (1981). He identified mesobeta-scale cyclonic circulations in film loops of visible satellite imagery. These MCVs were only apparent after the anvil debris from MCSs had dissipated or advected away. Johnston observed some vortices related to subsequent convection that occasionally produced severe weather (e.g., Hales 1990) and heavy rainfall (e.g., Fritsch et al. 1994).

[1] By "balance," we mean that the (assumed dominant) rotational part of the horizontal flow is to a good approximation related to the horizontal pressure gradient force through the nonlinear balance equation (Lorenz 1960; Charney 1955).

Corresponding author address: Diana L. Bartels, NOAA/ERL/NSSL/Mesoscale Research and Application Division, 325 Broadway, Boulder, CO 80303.
E-mail: bartels@mrd3.mmm.ucar.edu

FIG. 1. Visible satellite image shows midlevel vortex over eastern Colorado at 1831 UTC 9 June 1988.

These circulations can persist for several days (Johnston 1981; Bartels and Maddox 1991; Fritsch et al. 1994), going through several cycles of MCS–MCV regeneration.

Observational and modeling studies consistently reveal a three-layer structure in a mature MCS with the upper (near tropopause) layer and the boundary layer both characterized by shallow, cold, divergent anticyclonic circulations, while the midlevels are associated with a deep, cyclonic circulation (Maddox 1980, 1983; Cotton et al. 1989; Houze et al. 1989). A modeling study by Raymond and Jiang (1990) explains this observed MCS structure in terms of potential vorticity (PV) dynamics wherein the midlevels develop a positive PV anomaly and the lower and upper levels contain negative anomalies. The associated midlevel circulation (or MCV) is hypothesized to be the major organizational feature that lengthens the life of circular MCSs by enhancing the system's inertial stability (Ooyama 1982; Velasco and Fritsch 1987; Chen and Frank 1993).

Observations (Smull and Houze 1985; Leary and Rappaport 1987; Johnson et al. 1989; Jorgensen and Smull 1993) and numerical simulations (Zhang and Fritsch 1986, 1987, 1988a,b) have shown that the cyclonic circulation is generated within the stratiform precipitation region of convective complexes. Chen and Frank (1993) hypothesize that the local Rossby radius of deformation is decreased within the stratiform region to the extent that the system becomes dynamically large and inertially stable. Indeed, those vortices that are apparent in satellite imagery long after the convection has died are hypothesized to be quasi-balanced, inertially stable circulations. Their synoptic environments (characterized by weak midlevel flow and weak vertical shear) also contribute to their longevity.

Although MCVs have been receiving increased attention in the literature, detailed observations of their spatial and temporal structure have been primarily limited to special field programs [e.g., the Preliminary Regional Experiment for STORM-Central (PRE-STORM); Cunning (1986)]. Observational studies (Johnston 1981; Menard and Fritsch 1989; Johnson et al. 1989; Brandes 1990; Johnson and Bartels 1992; Fritsch et al. 1994) have shown that these vortices are at best barely detectable at the surface. The MCV is thus distinct from the ''wake depression'' (Fujita 1959), or wake low, which may coexist with or precede the MCV, as in Menard and Fritsch (1989) and Johnson et al. (1989). These studies have illustrated both common features of many MCVs and intriguing differences. Typical MCV diameter is 200–400 km. Maximum vorticity exists in midlevels (5–6 km) but extends through a deep layer of the atmosphere (3–9 km). As the vortices develop, the back edge of the stratiform echo often forms a hook-like structure, a feature first noted by Leary and Rappaport (1987). Available thermodynamic data are generally consistent with a warm core in midlevels. However, the complex thermodynamic structure noted by Brandes (1990) in his study of the 7 May 1985 vortex and Johnson and Bartels (1992) in their study of a 24 June 1985 MCV suggests that the term ''warm-core vortex'' may be an oversimplification. These two cases also differ in the primary source of their vorticity. Tilting of horizontal vorticity into the vertical appears to be dominant in the 7 May 1985 event (Brandes and Ziegler 1993), whereas Johnson and Bartels (1992) show that stretching was the dominant mechanism of the 24 June 1985 MCV.

Available data suggest that MCVs can be described as midlevel lenses of higher potential vorticity having mesoscale dimensions. This exercises a constraint on possible mechanisms for MCV formation since mesoscale creation and destruction of potential vorticity must be occurring as part of the formation process. Given the inadequacy of data available during formation of this particular MCV, we are obliged to concentrate on its structure after it is formed. We do, however, give an abbreviated description of the life history of the parent MCS.

2. Data and methodology

The MCV of 9 June 1988 is shown from a satellite perspective in Fig. 1. Profiler winds from Flagler, Colorado, and Fleming, Colorado, obtained within the stratiform region of the vortex-producing MCS and very near the center of the ensuing MCV, form the basis of this study. With the addition of satellite (including high-resolution rapid scan) images and Doppler and conventional radar data, this vortex was one of the best observed to date. Table 1 summarizes the various data used in this study, and appendix A describes the wind profiler data in more detail.

The MCV was first identified in visible satellite imagery and tracked using visible and infrared (IR) satellite images and available radar data. However, satellite imagery has serious limitations for MCV identification. For instance, visible data are not available

TABLE 1. Summary of special data.

Data type	Data period	Temporal resolution	Spatial resolution	
			Lower troposphere	Upper troposphere
Wind profilers[a]				
(50 MHz, two beam)				
Flagler (FLAG)	Entire period	Hourly averages	290 m (3.11–9.77 km MSL)	870 m (10.20–16.29 km MSL)
Fleming (FLEM)	Entire period	Hourly averages	290 m (3.27–9.93 km MSL)	870 m (10.08–16.16 km MSL)
NWS radar				
Limon (LIC) WSR-57[b] (10 cm)	Entire period Except 1430–1500 UTC	30 s–5 min	232-km range	2.5° horiz. beamwidth
Doppler radar CP-2 (10 cm)	1830–2254 UTC Except 2000–2100 UTC	6 min between base scans	225-km range at full PRF[c]	0.96° horiz. beamwidth
Satellite data				
Infrared	Entire period	30 min	8 km at subpoint	
Visible	1330–2300 UTC	15 min	4 km at subpoint	
Rapid scan	1830–2300 UTC	3–5 min	1 km at subpoint	

[a] Supplemental data from Platteville (50 MHz) and Denver (915 MHz) profilers were also examined.
[b] Additional 16-mm radar film from Alliance, Nebraska, and Goodland, Kansas, and radar logs from Cheyenne, Wyoming, were examined.
[c] Each volume scan began with a half pulse repetition frequency (PRF) scan, which effectively doubled the range.

at night, and the midlevel clouds that give clues to the existence of a circulation are often obscured by colder cloud tops in the IR data. To compensate, we have used time–height plots of profiler winds from all the Colorado sites to identify additional time periods when the profiler sites observed the vortex. Because of system evolution and propagation, the profiler time series alone cannot be used to unambiguously infer the character of the circulation. Hence, the integration of several data types was crucial to document the characteristics of this vortex and the convective system that generated it. Toward that end, the display capabilities of the Forecast Systems Laboratory advanced workstation (Bullock et al. 1988) enabled the convenient looping and overlaying of satellite (including rapid scan) and radar data for the 14-h period beginning at 1000 UTC[2] 9 June 1988.

These looped satellite, radar reflectivity, and Doppler velocity data together with Limon radar film were used to estimate movement of the MCS and to track the vortex center once it became apparent in the radar and satellite data. The track of the vortex center is shown in Fig. 2, together with locations of observing sites and surface topography. Until about 1600, the anvil debris associated with the MCS obscured the circulation center in the visible satellite data. Prior to 1600, the vortex track was based on radar data from Limon.

Confidence in the track improves between 1600 and 2300, a period during which the MCV was clearly discernible in both radar and satellite imagery and during which high-resolution rapid-scan satellite images were available. For this period we estimate a track[3] accuracy within 20 km. The vortex could not be tracked accurately after 2300 because the eastward-moving higher level anvil clouds associated with convection originating over the Rocky Mountains (apparent to the west of the vortex in Fig. 1) began to obscure the lower clouds associated with the MCV.

Our intent is to demonstrate that a reasonable horizontal MCV structure can be inferred from these profiler time series, despite slow changes in structure during the 10-h period. Consequently, we emphasize vortex-relative flow by removing the vortex motion and plotting profiler winds relative to the estimated MCV center at several profiler observation times. As a result, our analyses include a combination of temporal and spatial variations not completely distinguishable from each other. For a slowly changing feature, which we believe this vortex to be, this ambiguity leads to no significant problem. We use our derived spatial representation of the MCV to estimate horizontal and vertical tangential velocities, the vertical component of relative vorticity, and temperature and potential vorticity perturbations associated with a balanced vortex.

3. Synoptic-scale environment

The large-scale setting of the event is illustrated in the 500-mb analyses (supplemented by 6-km profiler

[2] All times are UTC. Subtract 7 h for LST.

[3] The track is assumed valid for 6 km MSL; this assumption places the MCV center east of Flagler at the time of closest approach (about 1630). If the track were assumed valid at 5 km, the center would be west of Flagler at 1630 because of a slight tilt in the vortex, discussed later.

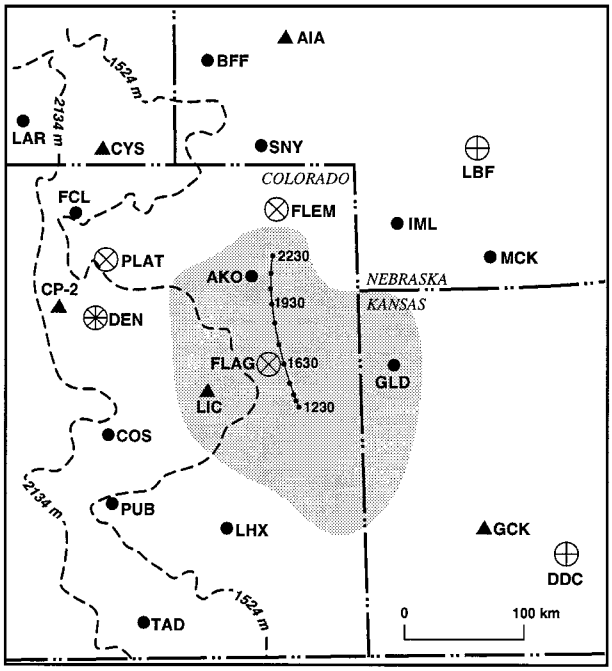

FIG. 2. Observational sites in the area of interest are shown. Dashed lines show the 1524- and 2134-m terrain contours. The solid line shows the estimated track of the center of the vortex with dots indicating the location of the center of the vortex at 30 min past the hour (UTC). The stippled area depicts the cold cloud shield contour (<-52°C) of the ''parent'' MCS at the time of maximum extent (0830 UTC). Surface stations are shown with solid circles, scanning radar sites are indicated by triangles, upper-air stations are indicated with an open circle enclosing a ''+,'' while profiler sites are shown by an open circle enclosing a ''×.'' The upper-air sites and LIC also made surface observations. The following station abbreviations are used: AIA—Alliance, AKO—Akron, BFF—Scottsbluff, COS—Colorado Springs, CYS—Cheyenne, DDC—Dodge City, DEN—Denver, FCL—Fort Collins, FLAG—Flagler, FLEM—Fleming, GCK—Garden City, GLD—Goodland, IML—Imperial, LAR—Laramie, LBF—North Platte, LHX—La Junta, LIC—Limon, MCK—McCook, PLAT—Platteville, PUB—Pueblo, SNY—Sidney, and TAD—Trinidad.

winds) for the period 0000 9 June–0000 10 June shown in Fig. 3. Throughout the period the predominant upper-air feature was a high-amplitude ridge. The fortuitously slow movement of the MCS and vortex is likely a result of the weak winds within the ridge.

The 500-mb analysis at 0000 9 June (Fig. 3a) illustrates the environment prior to MCS development. Short waves moving north, up the West Coast, and those moving south over the central United States interacted and caused the breakoff of the anticyclone over Colorado. During the period illustrated by Fig. 3, the anticyclone moves north-northeastward.

At 1200 9 June (Fig. 3b) the anticyclone is centered over northern Colorado. The MCV center is indicated just south of Flagler, Colorado. The 15 m s^{-1} wind observation at the Flagler profiler at 6 km is about twice the speed of the ambient wind flow over eastern Colorado. The easterly flow at Denver at 500 mb is part of a 1.5-km-deep layer apparently influenced by the vortex. Flow above and below this shallow layer had a southerly component, with a mean flow in the 3–10-km layer from 145° at 3.9 m s^{-1}, consistent with the location of the anticyclone to the north.

An explanation for the MCV's northward movement between 1200 and 2300 on 9 June, noted in Fig. 2, is elusive based on steering flow considerations alone. During this period the large-scale anticyclone moved toward the north at roughly twice the speed of the vortex. By 0000 10 June (Fig. 3c), the large-scale anticyclone has moved north-northeast, and a deformation zone separates the anticyclone from the ridge to the south. The vortex circulation at this time appears to be located along this deformation zone. Therefore, sometime between the synoptic observations, the background flow over east-central Colorado became more westerly. However, the crude resolution of the large-scale data coupled with the inherently weak winds characteristic of the synoptic environment lead to uncertainties concerning details of the temporal and spatial evolution of the background flow.

The ridging pattern is one of two characteristic patterns of the large-scale environment within which MCSs that spawn visually documentable MCVs develop (Bartels and Maddox 1991). This environment has weak midlevel flow and weak vertical and horizontal shear. Unique to this case, however, is the apparent absence of a readily identifiable upstream mid- to upper-level short-wave trough prior to the convective activity. The nearest clearly evident wave was located over Wyoming (see Fig. 3a). Other studies of midlatitude MCSs and, in particular, those that spawn MCVs (Menard and Fritsch 1989; Brandes 1990; Johnson and Bartels 1992) show associated short waves easily detectable in conventional data. The modeling studies by Zhang and Fritsch (1988a,b) and Chen and Frank (1993) demonstrate that short waves aid the spin-up of vortices. However, Johnson and Bartels (1992) and Chen and Frank (1993) suggest that a preexisting short wave is not a requirement for MCV development, as this case confirms.

Prior to MCS development, the surface winds (Fig. 4) indicate convergence over eastern Colorado. The surface dewpoints during the late afternoon ranged from 5°C (41°F) at Denver to 15.5°C (60°F) over western Kansas, with easterly upslope flow advecting moisture toward the west. In contrast, the air was hot and dry over southeastern Colorado. The Denver sounding at 0000 9 June (Fig. 5) shows a well-mixed lower troposphere with a nearly dry-adiabatic lapse rate from the surface up to 580 mb. This sounding is characteristic of the environment associated with high-based storms and the generation of evaporatively driven outflows (Brown et al. 1982). Although the surface air at Denver is dry, resulting in very modest instability for a surface-

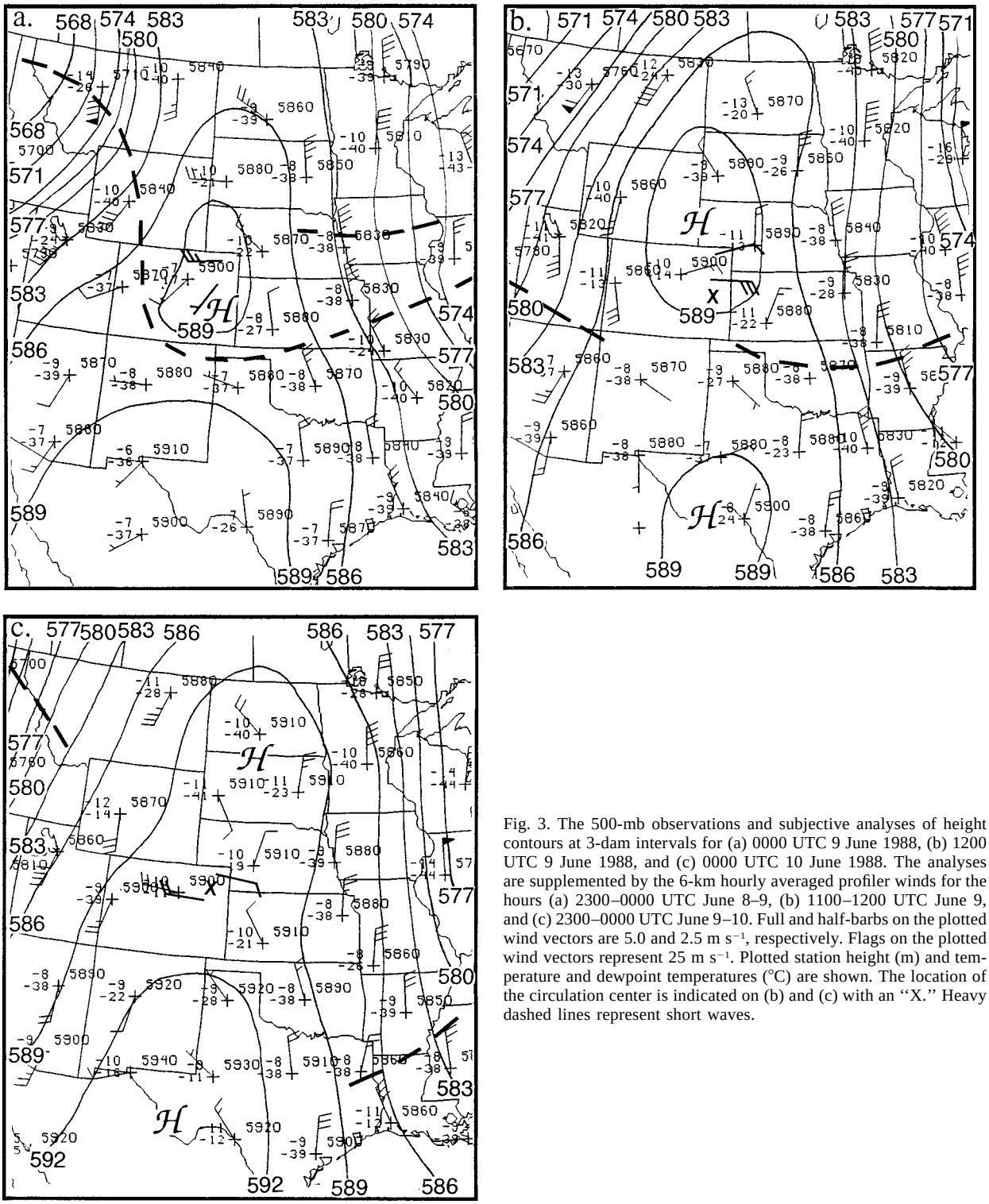

Fig. 3. The 500-mb observations and subjective analyses of height contours at 3-dam intervals for (a) 0000 UTC 9 June 1988, (b) 1200 UTC 9 June 1988, and (c) 0000 UTC 10 June 1988. The analyses are supplemented by the 6-km hourly averaged profiler winds for the hours (a) 2300–0000 UTC June 8–9, (b) 1100–1200 UTC June 9, and (c) 2300–0000 UTC June 9–10. Full and half-barbs on the plotted wind vectors are 5.0 and 2.5 m s^{-1}, respectively. Flags on the plotted wind vectors represent 25 m s^{-1}. Plotted station height (m) and temperature and dewpoint temperatures (°C) are shown. The location of the circulation center is indicated on (b) and (c) with an ''X.'' Heavy dashed lines represent short waves.

based parcel, surface conditions east of Denver show significant convective available potential energy (the hatched area on Fig. 5). Approximately 1–1.5 h after the balloon was released, two F1 tornadoes were observed 20–32 km northeast of Denver, as convection tapped the more unstable air to the east. This was the only severe weather reported in eastern Colorado that day.

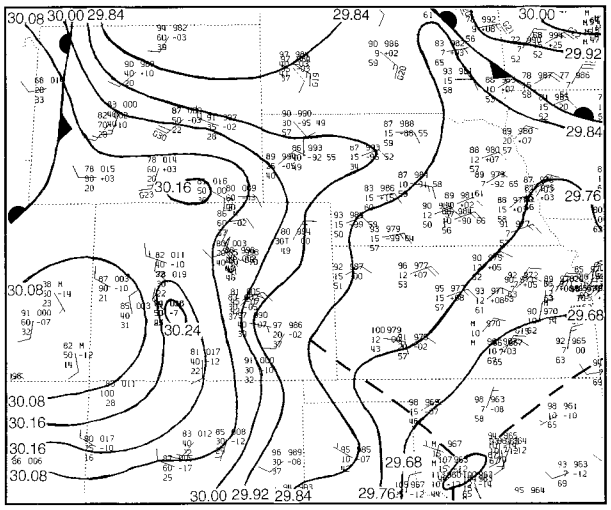

FIG. 4. Surface analysis for 0000 UTC 9 June 1988 in conventional (English) units. Isobars are shown for every 0.08 in. of mercury. Wind barbs as in Fig. 3.

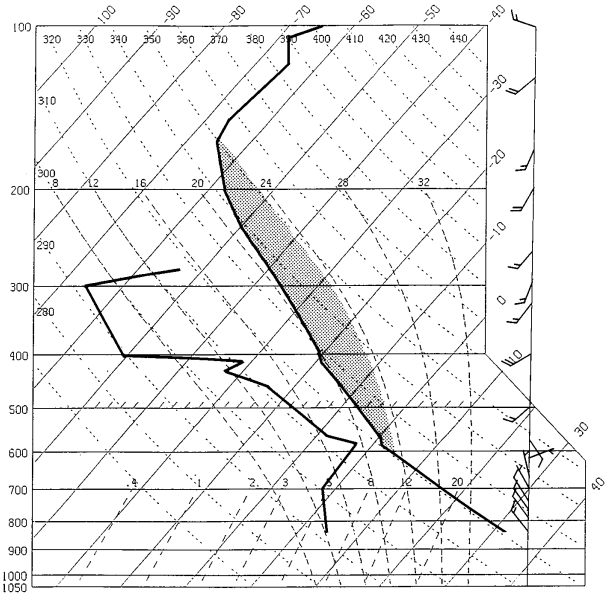

FIG. 5. Skew T–log$p$ plot of the Denver sounding at 0000 UTC 9 June 1988. Wind barbs as in Fig. 3. The hatched area indicates the positive area associated with a surface parcel in the moist air mass east of Denver.

4. The MCV life cycle

Profiler-measured airflow near and within the MCS and residual vortex is shown in the time–height series of Fig. 6. The satellite images in Fig. 6 give a snapshot of the ''parent'' MCS in early, mature, and early dissipating stages.

Convection over eastern Colorado began about 2000 8 June. This early period was characterized by several isolated storms, including a strong storm in the northeast corner of the state and the previously described tornadic storm northeast of Denver. The influence of the convection is first apparent in the profiler data as wind speed increases after 2230[4] UTC 8 June at Fleming (not shown) and after 0230 9 June at Flagler. The preconvective environment at Flagler was characterized by light southerly flow below 4 km and winds slowly veering with height above, implying weak warm advection. Above 6 km the speeds were generally less than 5 m s^{-1}. No obvious transitory features, such as mesoalphascale short waves, are apparent in the time–height series.

The sequence of base scans from the Limon WSR-57 show the vortex-producing convective system in more detail (Fig. 7). The system of interest had its origins in new echoes (denoted by arrows in Fig. 7a) located east of Limon and Flagler that are apparent in the 0215 scan. This area of new activity corresponds to the east–west band of cold cloud tops extending west from the Colorado–Kansas border in the 0300 satellite image (Fig. 6). These new echoes may have developed along outflow boundaries associated with the earlier strong convection located in northeast Colorado. [Surface observations indicated outflow boundary passage at Akron (AKO) at 0305 and Goodland (GLD) at 0325, where the winds shifted and gusted up to 17 m s^{-1}.] This new area of convection rapidly strengthened east of Flagler (Fig. 7b), as it evolved toward a bow-shaped line located on the Colorado–Kansas border at 0417 (Fig. 7c). This line persisted for the life cycle of the system. The entire system drifted slowly toward the southeast, with the line moving eastward more rapidly than the system as a whole. During its life cycle, however, the system only vaguely resembled a ''leading line with weaker echo trailing'' (Smull and Houze 1985) configuration characteristic of some organized convective systems.

The radar images show that the system underwent rapid modification during its life cycle. A new north–south line of intense storms (line 2 on Fig. 7d) formed south of Flagler within a region of light stratiform precipitation. Comparison with Fig. 6 indicates that the intense activity over Flagler is accompanied by a sharp windshift at midlevels (suggesting midlevel convergence) and brief enhancement of winds near the equilibrium level (suggesting upper-level outflow from the stronger convection to the south). The surface flow beneath the MCS is divergent, with outflow from the system reaching La Junta (LHX), well to the southwest of the MCS. The surface winds at La Junta measured 10.0–12.5 m s^{-1} for a continuous period from 0450 through 0750, with gusts of 15.0–17.5 m s^{-1}. Satellite images during this period (not shown) reveal the dominance of this new activity east of Limon as the cold cloud shield associated with the earlier strong storms erodes from the north.

[4] Times refer to the midpoint of the hour for which the hourly averages are derived.

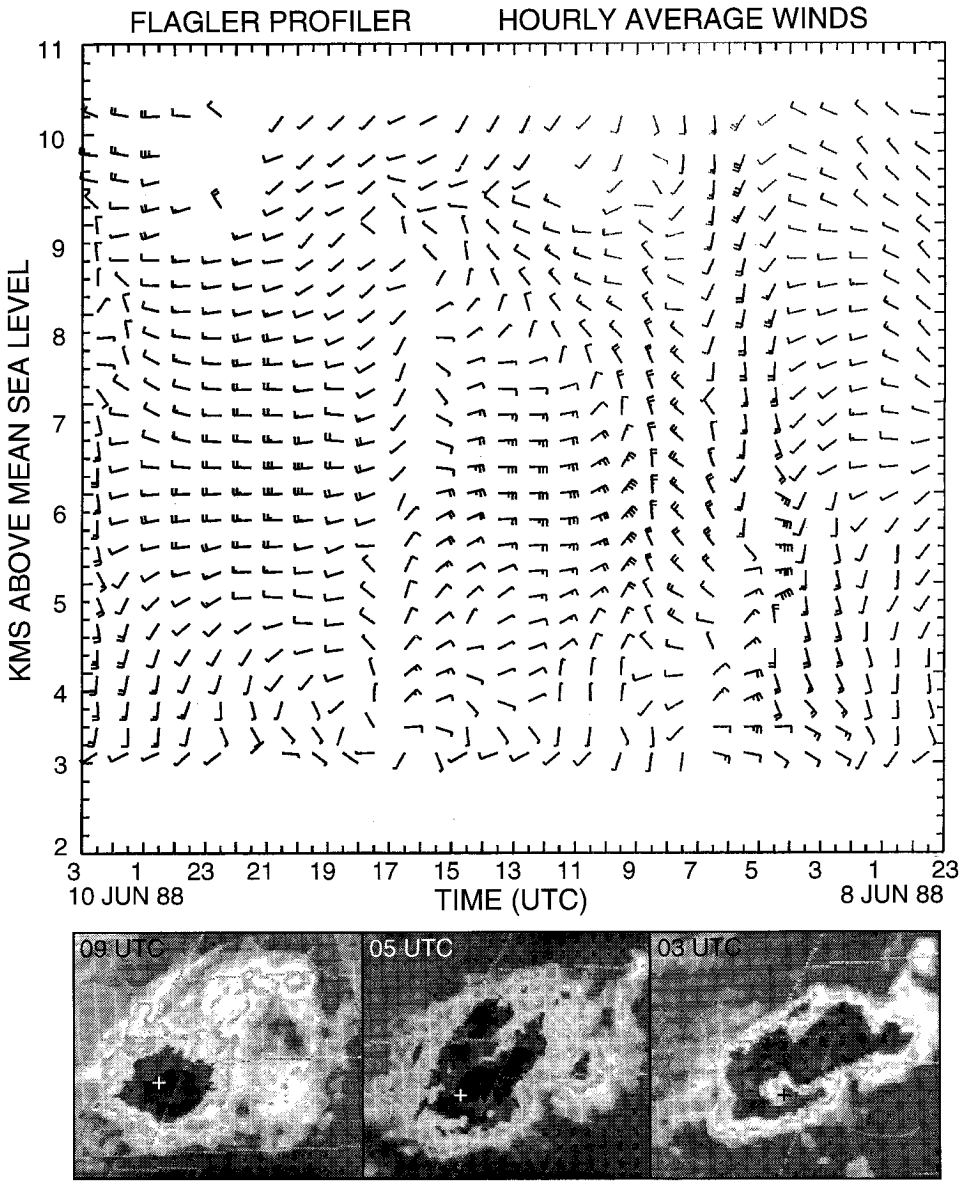

FIG. 6. Time–height series of hourly averaged profiler winds from Flagler. Wind barbs as in Fig. 3. Enhanced infrared satellite images at 0300, 0500, and 0800 UTC 9 June 1988 are shown below the time series with the location of Flagler shown by "+."

The Limon radar base scans beginning at about 0730 show a level-2 echo shaped like a cyclonically curved hooklike appendage. Over time, as the system dissipates, the echo takes on a cyclonically curved comma shape (e.g., Fig. 7i). The midlevel vortices studied by Leary and Rappaport (1987), Brandes (1990), Johnson and Bartels (1992), and Jorgensen and Smull (1993) were also characterized by a hooklike structure in the radar reflectivity data.

We speculate that the temporal veering of the midlevel winds at Flagler from northwesterly to northeasterly between 0730 and 0930 in Fig. 6 may result from a period of adjustment from a highly unbalanced state during the mature stage of the convective system toward a state of quasi-gradient balance hypothesized to exist later. Recall that by 0730 the deep convection near Flagler had ceased and radar echoes in the area were weak, but a thick anvil cloud was still in place. We do not believe that the process of downward transport of momentum and subsequent geostrophic adjustment envisioned by Stensrud et al. (1991) is acting in this case, since ambient flow aloft is very weak. However, the steep lapse rates and relatively dry conditions characterizing the environment of this MCS argue for the effectiveness of sublimation, melting, and evaporation in establishing a strong mesoscale downdraft as the convection south of

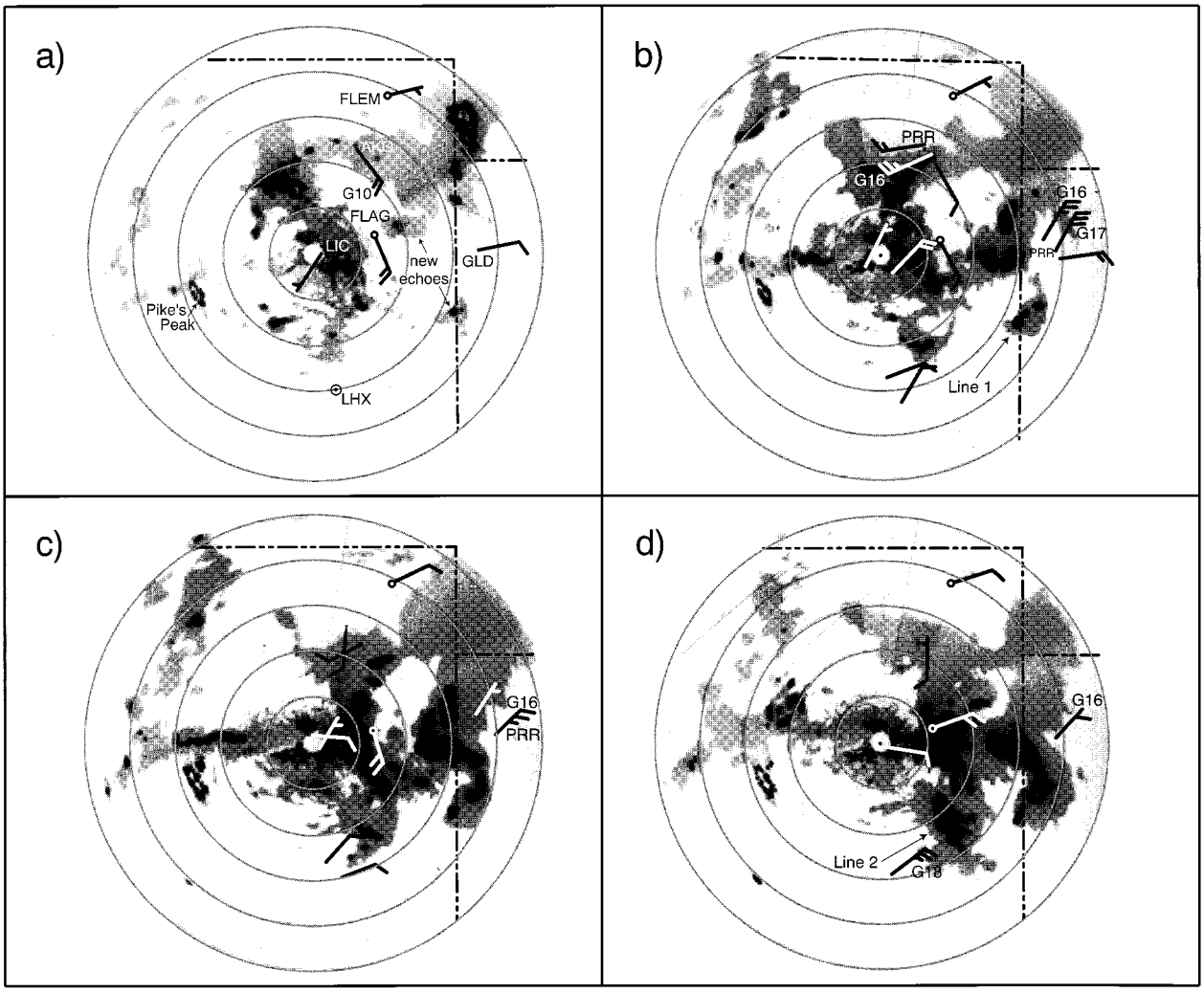

FIG. 7. Photographs of Limon WSR-57 radar base scans at (a) 0215, (b) 0335, (c) 0417, (d) 0517, (e) 0555, (f) 0628, (g) 0745, (h) 0825, (i) 0937, and (j) 1430 UTC 9 June 1988. State boundaries are overlaid. The range circles correspond to 46, 93, 139, 185, and 232 km. VIP levels 1 (<30 dBZ), 2 (30–40 dBZ), 3 (41–45 dBZ), 4 (46–49 dBZ), 5 (50–56 dBZ), and 6 (>57 dBZ) are indicated by the following gray scale: gray, white, black, gray, white, and black, respectively. Hourly averaged profiler winds from Flagler and Fleming at 4 km for the hour encompassing the radar observation are plotted. (The locations of Flagler and Fleming are indicated with open circles.) Surface winds (including gusts, m s^{-1}) and remarks of pressure rising rapidly (PRR) and pressure falling rapidly (PFR) are indicated for LIC, LHX, AKO, and GLD. Wind barbs as in Fig. 3. The locations of the hourly and special observations have been adjusted for differences in time of observation from the corresponding radar scan using a velocity vector of 5 m s^{-1} toward the southeast, representative of the overall MCS movement.

Flagler evolves into a large area of stratiform precipitation after 0700. We can only speculate, however, that convergence above this downdraft may have been sufficiently strong to spin up a vortex by stretching of the earth's vorticity.

At 1200, after the strong storms have died, cyclonic trajectories of reflectivity features are clearly revealed by Limon radar film. Visible satellite and CP-2 radar images during the morning and afternoon of 9 June show the distinct banded structure of the mature vortex seen first in the Limon radar base scans. Looped satellite imagery between 1545 and 2200 shows upper-level outflow bands above cyclonically rotating midlevel clouds. Before about 1900, the vortex appears approximately circular in satellite imagery (recall Fig. 1). As the day progresses, the vortex elongates along an east–west axis and drifts slowly to the north. This elongation may be a result of interaction with the deformation zone first apparent in the 0000 10 June synoptic data (cf. Figs. 3b,c).

The clouds within the vortex are never more than weakly convective, as inferred by cloud-top equivalent blackbody temperatures of near −20°C (~400 mb). The low reflectivities (20–30 dBZ) of the individual convective cells are also consistent with relatively low cloud tops (Fig. 8).

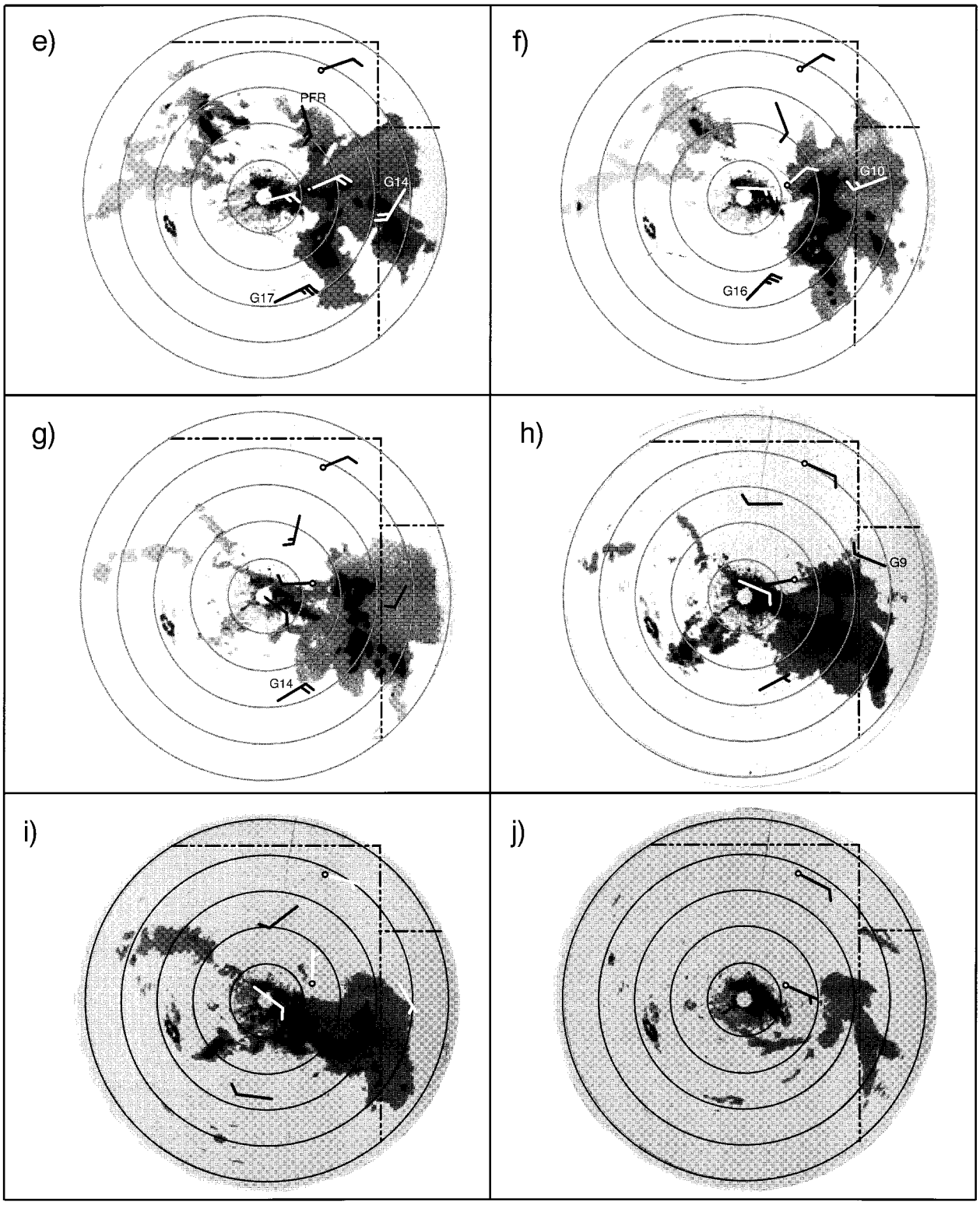

FIG. 7. (*Continued*)

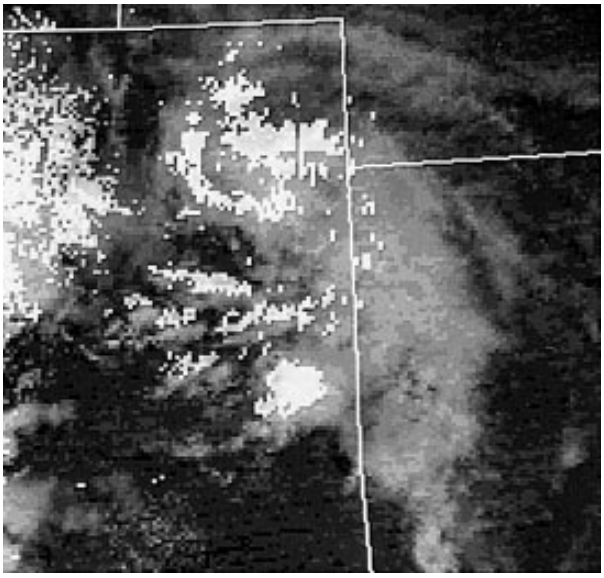

FIG. 8. Visible (1-km resolution) satellite image at 1945 UTC 9 June 1988 with CP-2 radar 0.2° elevation angle reflectivity image at 1948 UTC 9 June 1988 overlaid. The radar was operated in a one-half pulse repetition frequency (PRF) mode, which effectively doubled the range of the radar to 450 km. Reflectivities in the vortex were between 20 and 30 dBZ.

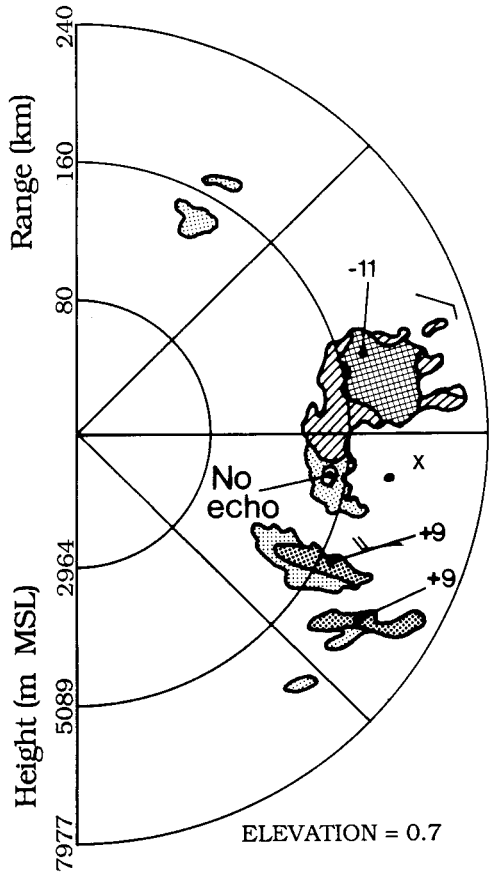

FIG. 9. Depiction of CP-2 Doppler radial velocities at 1830 UTC 9 June 1988. Negative (positive) values denote inward (outward) radial velocities. Single- and double-hatched areas approximate regions with radial velocities between 0 and -8 m s^{-1}, and less than -8 m s^{-1}, respectively. Light and dark stippling approximate regions with radial velocities between 0 and 8 m s^{-1}, and greater than 8 m s^{-1}, respectively. Range (km) and height of the center of the beam (m) as a function of range are indicated. Hourly averaged winds at 6 km from Flagler and Fleming (roughly the center of the pulse volume at that range) are indicated together with the location of the circulation center at 1830 UTC 9 June 1988. Wind barbs as in Fig. 3.

The radial velocity observations shown in Fig. 9 from CP-2 provide a quantitative measure of the circulation. For example, at 1848 the radial velocity pattern within the MCV is consistent with cyclonic rotation having a diameter of at least 100 km. At the range of the vortex, CP-2's 0.7° elevation beam has a depth of 3 km, with its midpoint located at 6 km above mean sea level (MSL). Radial velocities from the CP-2 radar are consistent with Flagler profiler observations averaged over the same layer.

The configuration and trajectories of radar echoes and clouds constitute strong circumstantial evidence of a vortex; the addition of profiler winds confirms the vortex existence. In the Flagler profiler time series (refer back to Fig. 6) easterly flow persists between 4 and 7 km MSL until 1530. Between 1530 and 1730, the easterlies rapidly change over to westerlies, first above 6 km MSL, then below. These changes are consistent with a northward-moving vortex that tilts slightly northwestward with height and whose center at 1630 is east of Flagler at lower levels, but west of Flagler at higher levels. Unfortunately, 5-min profiler data were not available to examine this 2-h time period in more detail.

The profiler observations indicate that before 1530, Flagler was in the northern branch of the vortex circulation. After 1730, when the vortex has drifted to the north, the Flagler profiler is in the southern branch of the circulation. For the next several hours the winds are steady, with midlevel speeds exceeding 15 m s^{-1} between 1930 and 2130. Finally, by 0230 UTC 10 June midlevel westerly flow is not observed at Flagler, suggesting that the vortex was no longer influencing winds over Flagler.

Using this time series and extrapolating the vortex track in Fig. 2 to 0230 UTC 10 June indicates a vortex radius of just over 150 km. This estimate compares with the satellite-determined vortex radius of 125 km. We note that it is common for vortices to have a ''kinematic'' dimension that is somewhat larger than that implied by the clouds alone (Menard and Fritsch 1989; Bartels and Maddox 1991; Wang et al. 1993).

Although both Platteville and Stapleton profilers were northwest of the generating MCS and west of the MCV (as defined by satellite), time–height plots of winds at these sites (not shown) suggest that they were influenced by the vortex early in the morning. Later, the Platteville and Stapleton profiler observations were affected by the airflow associated with the new day's heating-induced

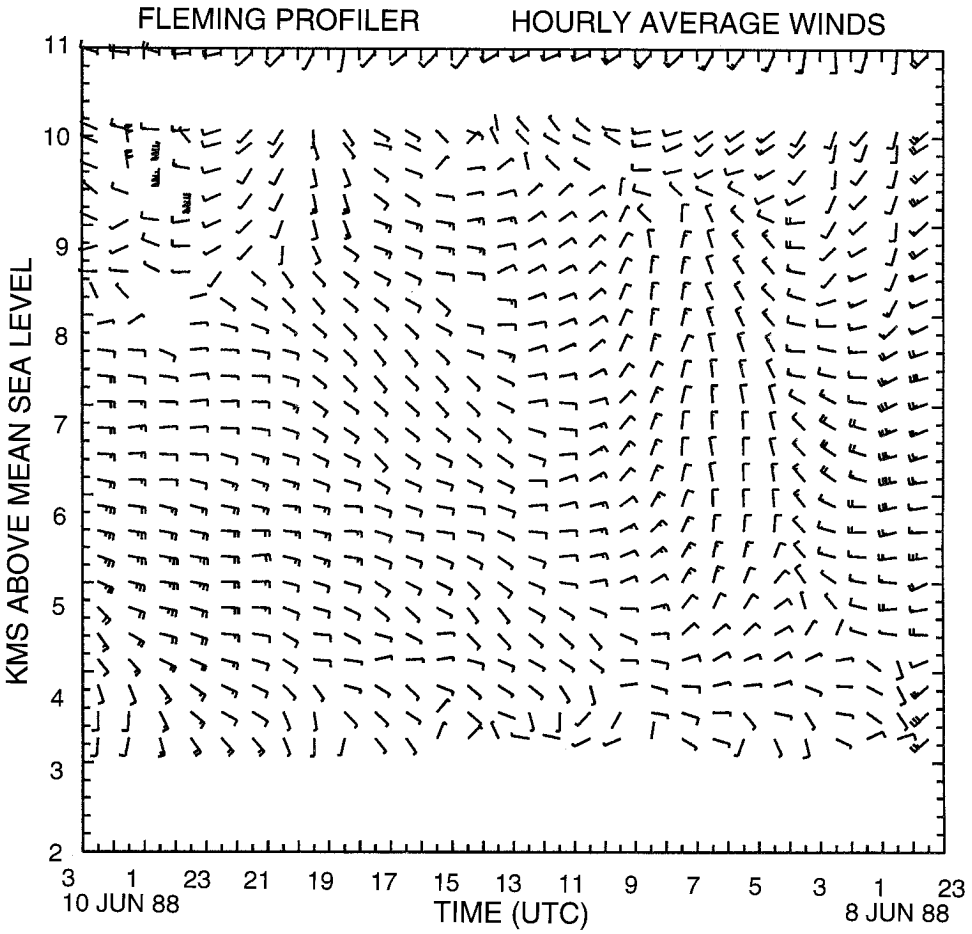

FIG. 10. Profiler time–height observations from Fleming. Wind barbs as in Fig. 3. The obviously erroneous winds at 2330 UTC 9 June and 0130 UTC 10 June 1988 between 9 and 10 km are retained for completeness.

convection over the mountains, and any influence of the vortex was obscured. Fleming, on the other hand, was located near the northern edge of the anvil and north of the precipitation echoes associated with the vortex-generating MCS. Later in the day, as the vortex moved north, Fleming apparently sampled the airflow within the MCV. A layer of easterly flow is observed at Fleming beginning at 1030 (Fig. 10). This easterly flow is much weaker than at Flagler, however, and shows influence from the flow around a synoptic-scale high pressure system centered in southeast Wyoming at 1200 (recall Fig. 3b). (Note that the midlevel winds at Fleming shifted from westerly to northerly to easterly prior to 1200 UTC 9 June, reflecting the movement of the synoptic-scale anticyclone from a location south, then east, and finally north of Fleming.) As the vortex moves north, the easterly flow strengthens and deepens in a vertically expanding layer after 1830, when the MCV center is within 100 km of the Fleming profiler. Loops of the CP-2 reflectivity and velocity data also indicate the northern portion of the vortex near Fleming by 1830, suggesting that intensifying easterlies at Fleming are the counterpart of the vertically expanding easterlies observed at Flagler earlier.

Surface pressure traces at Limon and Akron (not shown) show little reflection of the vortex. The absence of a surface pressure reflection of the vortex has been a consistent finding of MCV investigations (Brandes 1990; Menard and Fritsch 1989; Johnson and Bartels 1992; Fritsch et al. 1994).

The last available CP-2 radar depiction is at 2254. After this time the less sensitive WSR-57 radar at Limon provided the only radar coverage of the vortex. By 0130 UTC 10 June shallow and weak bands in the southern portion of the MCV were out of the Limon radar's view. Subsequent evolution of the vortex is therefore uncertain.

5. Diagnosis of vortex structure

The three-dimensional wind structure of the vortex is diagnosed in this section. Vortex-relative winds were determined by subtracting the northward vortex motion (which averaged 5 m s^{-1}) from the ground-relative pro-

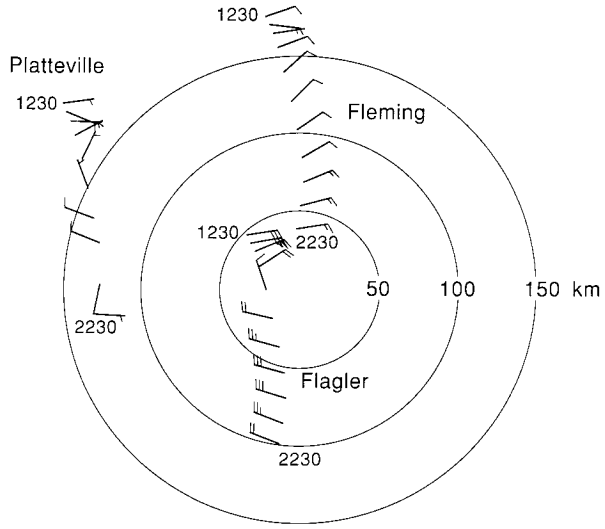

FIG. 11. Relative winds plotted relative to the vortex center at 6 km MSL derived from Flagler, Fleming, and Platteville profiler observations for each hour between 1230 and 2230 UTC, as indicated. Wind barbs as in Fig. 3.

filer winds and then plotting the resulting winds relative to the center of the moving vortex. Since the vortex moved slowly, the relative winds are very similar to the observed winds, except close to the vortex center. Strictly speaking, the horizontal structure inferred from the profiler time series is only correct if the vortex is steady. According to our analysis a steady-state assumption is best satisfied between 1200 and 2300; after 2300 the vortex center could not be accurately tracked with the available data.

The spatial representation of the steady-state vortex is shown in Fig. 11 at 6 km MSL, the height of maximum rotation. It clearly shows a cyclonic circulation. At Platteville, located north and west of the clouds associated with the vortex, the relative winds between 1230 and 1930 are consistent with the cyclonic circulation. After 1930, however, the winds at Platteville become variable, probably due to nearby convection.

Vortex-relative winds at 5 and 7 km MSL (not shown) reveal the modest tilt of the MCV center to the west-northwest with height. A tilting vortex is not unique to this case (Johnson and Bartels 1992; Zhang and Fritsch 1988b). However, without a better quantitative description of the slope we have chosen to perform subsequent analyses assuming a circular vortex with no tilt. Close to the center, vortex-relative tangential winds V_t are sensitive to relatively small differences in center placement and the assumption of a vertical vortex. Beyond 50 km, however, the Flagler and Fleming profiler observations are almost directly north or south of the MCV center, and the relative winds are approximately tangential. As a result, V_t is not significantly affected by either vortex tilt or placement.

Views of the vertical structure of the vortex are afforded by the selected profiles of V_t in Fig. 12. Each profile, whether north or south of the vortex center or whether made at Flagler or Fleming, shows remarkably similar structure: tangential winds exceeding 5 m s^{-1} between 5 and 7 km with a distinct maximum near 6 km MSL. The most significant difference between the profiles is found above 7 km, where larger relative wind speeds exist in the south (or later) profiles observed by the Flagler profiler. Taken together, these profiles suggest substantial vortex symmetry, at least in the north–south plane. Symmetry is also suggested by the closely matching radial profiles of V_t exhibited by 6 km MSL Flagler observations in Fig. 13, where the segments from 1230 to 1630 and 1630 to 1830 are located north and south, respectively, from the vortex center. We view this agreement with caution, however, given the previously described sensitivity of the close-in V_t calculations to small errors in the vortex center locations.

Although the general structure of the winds both north

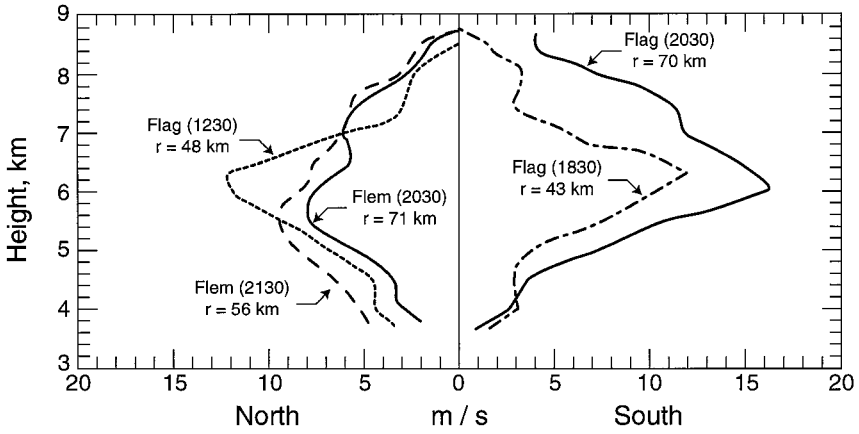

FIG. 12. Profiles of tangential wind (m s^{-1}) at various locations relative to the vortex center (refer to Fig. 11 for reference locations). All speeds are positive and represent cyclonic rotation. Distances from the vortex center and observation times are indicated. The profiles in the right (left) halves of the plot are located south and (north) of the vortex center.

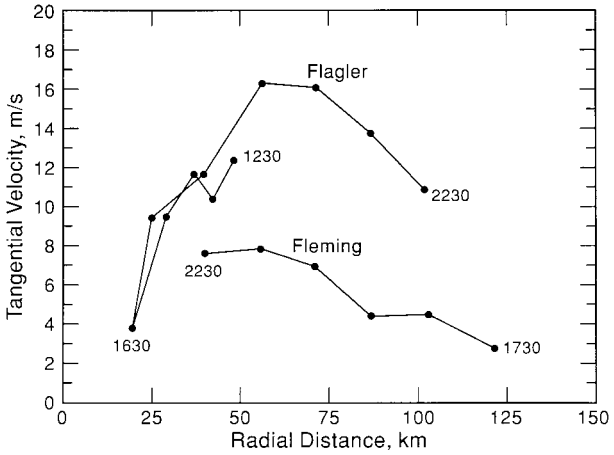

FIG. 13. Tangential winds (m s^{-1}) at 6 km MSL at various radial distances from the vortex center. Positive values represent cyclonic rotation. The first and last observation times for each curve are indicated; points in between show successive hourly averages. All the Fleming observations and those from Flagler before 1630 UTC describe conditions north of the vortex center; after 1630 UTC the Flagler winds are located south of the vortex center.

and south of the center display symmetry, closer examination of the Flagler and Fleming profiles in Fig. 12 reveals substantial asymmetry in tangential wind magnitudes. These simultaneous profiles were coincidentally located about 70 km north and south, respectively, of the MCV center. Because of this fortuitous timing, they isolate spatial differences between the northern and southern branches of the vortex circulation from temporal ones.[5] Of course we cannot say what this comparison would have shown earlier, but at 2030 the maximum in the southern branch is twice as large as that of the northern branch and perhaps 0.5 km higher. For reasons described previously, we are unable to convincingly separate actual MCV asymmetries from north–south variation in the background zonal wind.

The set of vertical and horizontal profiles in Figs. 12 and 13 also give a confusing picture of another vortex characteristic, its steadiness. Examination of the hour-by-hour Flagler profiles (not all shown) suggests only minor changes in the assumed structure at points within the vortex separated by a few tens of kilometers, consistent with a steady-state assumption. The dashed curves on the left portion of Fig. 12 also leave an impression of steadiness. These two Flagler and Fleming V_t profiles were made in very nearly the same location relative to the MCV (about the same radial distance north and northwest of the center, and separated in system-relative space by only 30 km), but they are temporally separated by 9 h. Thus, their similar structure suggests only slow change in MCV structure over time.

[5] We ignore slight MCV-relative location differences caused by the 1-h averaging period required for the observations.

This apparent steadiness is called into question, however, by the relatively small magnitudes of the tangential velocity measured at Fleming (Fig. 13). If the vortex is radially symmetric or symmetric about an east–west axis, then the differences in magnitude near 50 km between the Flagler (southern branch) and the Fleming (northern branch) profiles indicate a temporal change in overall tangential velocity between the early hours of the track and the later. (We note in this respect that some of the apparent reduction in velocity in the Fleming profile is a result of the choice of 6 km for the profile height; as Fig. 12 shows, we thus catch the Flagler vertical profile at its maximum but miss the physically lower maximum at Fleming.) On the other hand, Fig. 13 might also be interpreted to indicate a steady asymmetric vortex (or a vortex that is being slowly sheared apart by weak deformation in the larger-scale flow), with stronger velocities to the south, as suggested by the profiles in Fig. 12. This interpretation, however, is also subject to question. If the vortex were both balanced and asymmetric, an asymmetric distribution of potential vorticity is implied. Thus, there will be horizontal advection of potential vorticity, resulting in some degree of nonsteadiness.

The evidence for steadiness and symmetry is thus somewhat contradictory. Since our analysis cannot demonstrate steadiness without assuming symmetry (or vice versa), and since the observations are not adequate to describe a definitive ambient flow, we are left with some uncertainties in both respects. Our best judgment is that the vortex itself is sufficiently steady to be considered to be in a quasi-balanced state and that there exist substantial north–south spatial variations in the MCV that are larger than temporal ones.

We can extend the V_t calculations to estimate the average vertical vorticity, ξ_m, of the mature MCV inside the radius of maximum wind, r_m (i.e., within 75 km of its center). Since r_m may vary with direction from the center, the most general description of ξ_m is

$$\xi_m = \frac{1}{A_m} \oint_C \mathbf{V} \cdot d\mathbf{l}, \tag{1}$$

where $\mathbf{V}$ is the horizontal velocity vector, $d\mathbf{l}$ is a directed line segment along C, and A_m is the area enclosed by the curve C. The profilers at Flagler and Fleming at 2030 are ideally placed to describe simultaneously the tangential wind and radius of maximum wind north and south of the circulation center. Since there are no observations east and west of the vortex center, we assume radial symmetry of V_t and a circular vortex. (Thus, V_t at Flagler and Fleming at 2030 were averaged.) The resulting profile of ξ_m is shown as the curve in Fig. 14. At 6 km the magnitude of ξ_m exceeds three times the local Coriolis parameter.

An independent estimate of the circulation can be made using the field of vectors (not shown) determined by manually tracking radar reflectivity patterns and sat-

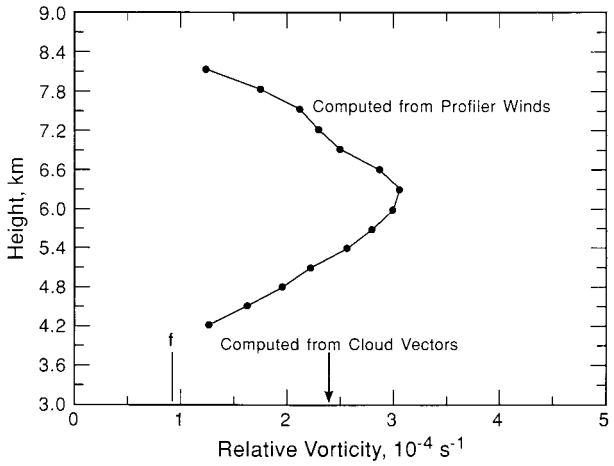

FIG. 14. Profile of average relative vorticity (10^{-4} s^{-1}) at the radius of maximum wind (70 km), computed using an average of Flagler and Fleming's 2030 UTC profiler winds. The local value of the Coriolis parameter f and the midtropospheric vorticity computed from radar reflectivity and satellite cloud tags are also indicated.

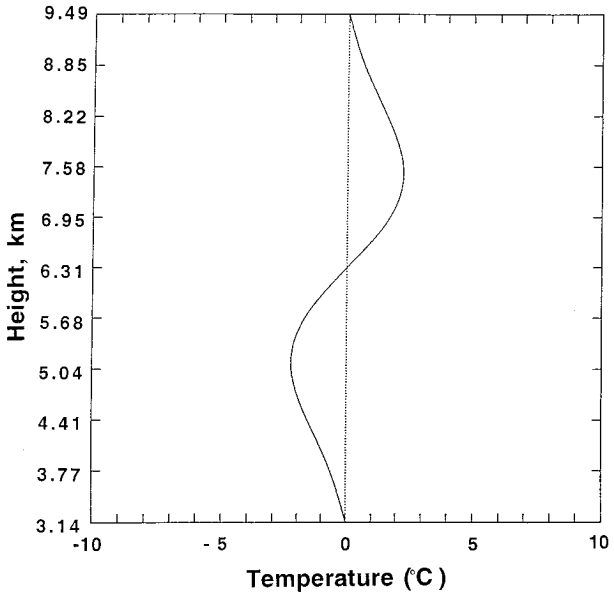

FIG. 15. Profile of modeled temperature perturbation (°C) valid for the center of the vortex.

ellite-observed cloud features within the midtropospheric layer of the MCV for each satellite and radar image. When located relative to the vortex center, these vectors by themselves qualitatively suggest an elliptically shaped vortex with an east–west major axis. Unfortunately, the paucity of vectors beyond 70 km to the northwest and southwest of the center complicates the determination of r_m required for quantitative determination of ξ_m. Thus, we assume circularity, as before, and compute the average V_t using all the radar- and satellite-derived winds in the circular annulus between 50 and 100 km. Since ξ_m so computed (indicated on Fig. 14) is likely to be representative of some sort of vertical and horizontal average, it is not surprising that its magnitude is less than the maximum computed using the vertically detailed profiler observations.

In the next section we further extend these vorticity calculations to infer a temperature and potential vorticity structure for the vortex, assuming for simplicity that it is vertically oriented and axisymmetric. The resulting temperature and potential vorticity perturbations are therefore likely to represent an upper bound on the magnitude of the true perturbation.

6. Modeled temperature and potential vorticity perturbations associated with the vortex

The duration of the MCV and the apparent dominance of vorticity over divergence in the vortex core region (100-km radius) suggest that the flow in the vortex is in an approximately balanced state for several hours following 1200 9 June. It is therefore possible to calculate the virtual temperature perturbation necessary to support the observed tangential velocity distribution by assuming gradient wind balance in the radial direction. For simplicity the vortex is modeled as an inner core of solid rotation of radius 70 km with no tilt in the vertical, surrounded by an outer region having zero absolute vorticity at the level of maximum wind. The assumed vertical profile of vertical vorticity in the model vortex is a cosine-squared function fit via least squares to the profile of Fig. 14. Other details of the calculation of the virtual temperature perturbation are given in appendix B.

The resulting virtual temperature perturbation at the center of the model vortex is depicted in Fig. 15. The vortex is cold core below the level of maximum tangential wind and warm core above, with an amplitude of 2.3°C. In Fig. 16 this perturbation (assumed to be entirely in temperature rather than mixing ratio) is shown superposed on a sounding horizontally interpolated from neighboring soundings to the 2030 location of the vortex. (Details of this interpolation process are also given in appendix B.) The strong stable layer spanning the vertical core of the vortex near 500 mb, with cooling below and warming above, is often found in soundings taken in dying MCSs or near confirmed MCVs [e.g., Fig. 35 of Leary and Rappaport (1987) and Figs. 15 and 16 of Bartels and Maddox (1991)]. However, the cold cores in these two examples are centered near 600 mb, somewhat lower than the 525-mb cold-core center determined here.

We show the structure of potential vorticity in the center of the modeled MCV in Fig. 17. Details of the calculation of potential vorticity, which incorporates virtual temperature effects, are discussed in appendix B. The resultant PV profile looks very similar to that diagnosed by Fritsch et al. (1994) for a mature MCV. A possible interpretation of Fig. 17 is that the MCV is a thin lens of high potential vorticity centered near 450

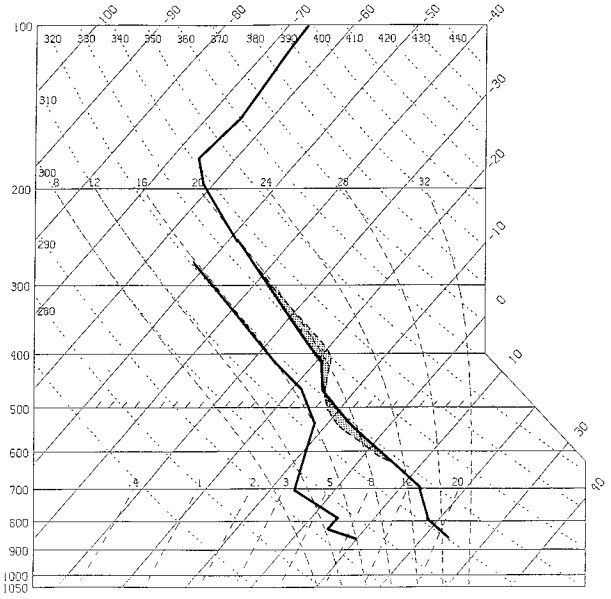

FIG. 16. Skew *T*–log*p* plot showing interpolated sounding at 2030 UTC at the center of the MCV (solid line) with assumed temperature perturbation (dashed line) from Fig. 15 superposed.

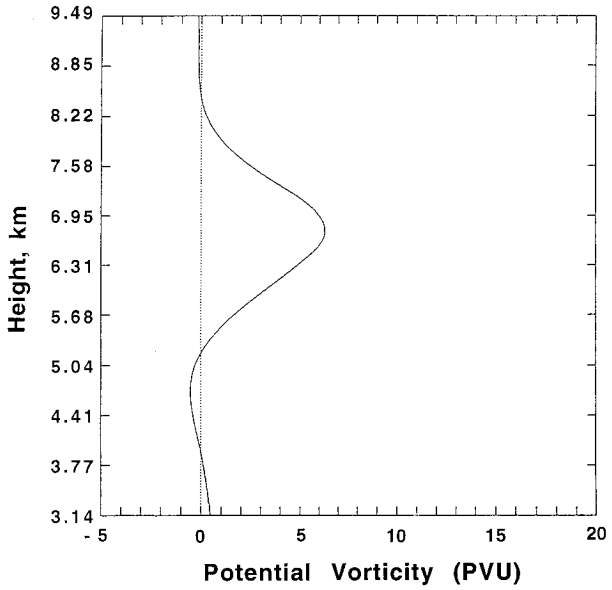

FIG. 17. Profile of modeled potential vorticity structure valid for the center of the vortex. Units of potential vorticity are 10^{-6} m^2 K kg^{-1} s^{-1}.

mb and generated by phase change processes (condensation, evaporation, sublimation, etc.) in the previous night's MCS. Note that there has been a corresponding reduction of potential vorticity in a fairly deep layer above and below this lens.

The PV volume integral conservation relation of Haynes and McIntyre (1987) can in principle be applied to the change of this PV distribution from an initial, pre-MCS background field (C. Davis 1996, personal communication). Considering only the layer between roughly 700 and 300 mb shown in Fig. 17, the decrease in PV above and below the vortex is insufficient to compensate for the increase in the vortex itself. This discrepancy is consistent with the speculation made earlier that the assumption of circular symmetry overestimates the relative vorticity of Fig. 14. However, midlevel isentropic velocity convergence, typical in MCSs, may also have contributed additional PV.

7. Discussion and conclusions

This study was motivated by the fortuitous development of a convectively generated vortex over an array of profilers in northeast Colorado. Combined with good supporting data (primarily satellite and radar), these observations offered a look at the internal structure of these mesoscale phenomena.

The parent convective system developed within the quiescent large-scale setting of a high-amplitude ridge axis. The first evidence of vortex development within the stratiform area of the system was noted shortly after convection within the system began to decline. The vortex persisted for at least 12 h after its first observation. In its first few hours of development it likely moved very slowly southeast, along with the stratiform region in which it developed. Near sunrise, however, the vortex changed direction and moved more rapidly to the north-northwest. Other investigators (Fritsch et al. 1994) have noted that vortices often increase their speed after the dissipation of the parent system, which tends to occur near sunrise. It is unusual, however, for a vortex to move in a direction opposite to that of the generating MCS. Available data did not provide clear information on the demise of the vortex.

Our study reveals the following salient characteristics of this event.

1) The parent MCS formed in a very weakly sheared, nearly barotropic environment.
2) Though radar depictions show that the MCS was composed of several poorly defined bands of convection, the cloud shield of the MCS took on a circular, symmetric character late in its lifetime.
3) The vortex was of mesobeta scale, yet exhibited an impressive degree of steadiness and circularity. This argues that the vortex was in a state of balance, with the attendant cold core below about 6 km and warm core above, and an intervening thin lens of large potential vorticity.

There exists insufficient information to diagnose the origins of this vortex. This is unfortunate, since no dominant theory for the formation of such vortices has yet emerged. Because this vortex formed in an environment of weak ambient wind shear, arguments based on tilting of ambient horizontal vorticity are less convincing than in other documented cases. Vertical stretching of am-

bient vertical vorticity is a likely contributor, since the strong divergence at the surface and the existence of a substantial upper cloud shield as detected by the IR imagery do give evidence for the three-layer structure of midlevel convergence surmounted above and below by layers of divergence. Whether this together with the scale contraction produced by advection in a flow field exhibiting convergence can account for both the intensity (amounting to a factor of 4–5 over the ambient absolute vertical vorticity) and small size of the vortex is uncertain. The strong perturbation of the profiler winds following the passage of the convective line (Fig. 6) plus the strength of the low-level outflow suggest that the system itself generated substantial horizontal vorticity by baroclinic processes. It is tempting to speculate that tilting and subsequent stretching of this MCS-generated horizontal vorticity may also have contributed to vortex formation (Skamarock et al. 1994).

In any event, the evidence strongly supports the existence of a lens of high potential vorticity in the midtroposphere. We note that if this lens was produced by diabatic rather than frictional processes, we must consider that sublimation, evaporation, and melting processes must have been very important because of the dry environment in which the system formed. Further, these would have likely been the dominant diabatic processes during the period and in the region of formation. The location of the potential vorticity lens at a height well above the melting level argues, however, that if melting was important, subsequent upward advection must have occurred.

Other important questions remain. What is the fate of the vortex after it is obscured from satellite view by the anvil of the adjacent convection? Is the demise of such vortices due to the stretching of their PV lenses by the large-scale deformation field? Why is the vortex elongated in the east–west direction and how does the elongation change with time? Why are velocities in the southern part of the vortex so much stronger than those in the northern half? Is there internal gravity wave activity superposed on the overall balanced flow that can account for the asymmetries?

Acknowledgments. We thank John Augustine, David Merritt, and John Smart of Environmental Research Laboratories for assistance with obtaining data. Forecast Systems Laboratory provided extensive use of its workstation. Zewei Lu of the National Natural National Science Foundation of China helped with the formulation of the potential vorticity calculation. A portion of this work was included in the masters thesis of DLB at the University of Oklahoma. Hence, DLB acknowledges her thesis committee: R. Maddox and Professors H. Bluestein and F. Carr. Thanks also to Brad Colman (National Weather Service), Chris Davis (National Center for Atmospheric Research), Carl Hane (National Severe Storms Laboratory), Robert Maddox (National Severe Storms Laboratory), Dave Rust (National Severe Storms Laboratory), and Ed Szoke (Forecast Systems Laboratory) for helpful comments and/or reviews of various versions of this paper.

APPENDIX A

Profiler Data Used in This Study

The now defunct Colorado wind profiler network, which provided the data used in this study, consisted of three VHF 50-MHz Doppler radars located near Platteville, Flagler, and Fleming, and one UHF 915-MHz system collocated with the Denver radiosonde site at Stapleton International Airport northeast of Denver. The station locations are indicated in Fig. 2. All profiler data shown are hourly consensus average winds from these sites. The hourly averaged winds were derived from raw data consisting of radial velocity measurements obtained over a 5-min sampling period. The consensus averaging process is described by van de Kamp (1988). All profiler observation times refer to the time of the midpoint of each hour.

Details of the radar's design and operation are given by Strauch et al. (1984). Table 1 summarizes characteristics of the profiler data used here. Note that the Flagler and Fleming observations were not available at identical heights but were offset by 0.12–0.17 km. The height of the lowest gate is 1.5 km above ground level. Since MCVs are primarily a midtropospheric phenomenon, the lack of low-level data was not critical to this study.

Since the radar's oblique beams were centered about 15° from the zenith, the volumes sampled by the oblique beams at a particular range gate are separated by roughly $h\sqrt{2}/4$, where h is the height above ground of the gate. Thus, at 8-km height, the volumes the oblique beams sampled were separated by about 3 km. This distance pushes the limits of the fundamental assumptions required for the computation of valid horizontal winds, which are homogeneity in space and the absence of strong vertical motion of reflectors. [See Weber et al. (1992) for further discussion.] Obviously, these wind profilers cannot measure representative winds in a strongly convective environment, where air motions are not uniform in space or time and where strong vertical motion exists. Because Flagler and Fleming do not have vertically pointing beams to determine vertical motion, horizontal velocity is computed assuming zero vertical velocity. Augustine and Zipser (1987) discuss the two-beam 50-MHz profiler's utility in sampling mesoscale convective systems and note that the lack of a vertical beam is somewhat mitigated by the long (1 h) consensus averaging period. They also emphasize that the two-beam 50-MHz radars (unlike the 405-MHz radars) were not adversely affected by light to moderate precipitation.

APPENDIX B

Temperature and Potential Vorticity Calculations and MCV Sounding Interpolation Procedures

The expression for gradient wind balance in an axisymmetric vortex may be written as

$$V_\theta = \left(\frac{fr}{2}\right)(S - 1), \tag{B1}$$

where V_θ is the tangential velocity, $S = [1 + (4/f^2 r)(\partial\Phi/\partial r)]^{1/2}$, r is the radial distance from the center of the vortex, Φ is the geopotential height, and f is the Coriolis parameter (McWilliams 1988). For convenience we adapt use of the vertical pressure coordinate (Phillips 1973)

$$Z = \left(\frac{-RT_o}{g}\right)\ln\left(\frac{P}{P_o}\right), \tag{B2}$$

where $P_o = 1074$ mb and T_o is 262 K. Here, Z has units of height, and the values of P_o and T_o are chosen to best approximate the geopotential height through the depth of the vortex.

The gradient thermal wind equation can then be written as

$$\frac{\partial V_\theta}{\partial Z} = \left(\frac{1}{FS}\right)\left(\frac{\partial T}{\partial r}\right), \tag{B3}$$

where $F = fT_o/g$. This equation forms the basis for calculation of the temperature perturbation.

We assume that V_θ can be expressed in separable form as $V_\theta = V_m(Z)\Re(r)$. By expressing V_θ in this way we are modeling the MCV as an upright axisymmetric vortex whose tangential velocity displays the same functional form with respect to r at all heights. The assumed functional form for $V_m(Z)$ is

$$V_m(z) = \begin{cases} V_{\max}\cos^2\left[\left(\frac{\pi}{D}\right)(Z - Z_{\max})\right], \\ \quad Z_{\max} - \frac{D}{2} \le Z \le Z_{\max} + \frac{D}{2} \\ 0, \text{ otherwise} \end{cases} \tag{B4}$$

where $V_{\max}$, D, and $Z_{\max}$ are chosen on the basis of a least squares fit of (B4) to the system-relative tangential velocity at a radius of 70 km, obtained by averaging the 2030 UTC system-relative tangential component of velocity from the Flagler and Fleming profilers (see Fig. 12). The resulting vertical profile of tangential velocity at the 70-km radius of maximum wind is depicted in Fig. B1.

The functional form for $\Re$ is

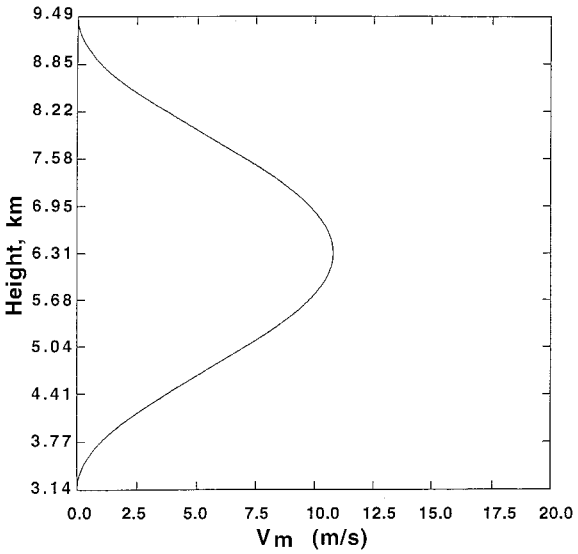

FIG. B1. Profile of modeled tangential velocity (m s^{-1}) structure valid for the center of the vortex. The values used to solve Eq. (B4) were $V_{\max} = 10.8$ m s^{-1}, $Z_{\max} = 6.31$ km, and $D = 6.35$ km.

$$\Re = \begin{cases} \frac{r}{r_m}, & r < r_m, \\ (B + 1)\left(\frac{r_m}{r}\right) - B\left(\frac{r}{r_m}\right), & r_m < r < R', \\ 0, & R' < r, \end{cases}$$

where

$$B = (1/2)(fr_m/V_{\max}). \tag{B5}$$

This corresponds to solid rotation in the core ($r < r_m$) and a $1/r$ dependency (modified by the Coriolis term) outside. The quantity R' is the radius at which V_θ decreases to zero under the constraint that the vertical component of absolute vorticity is zero outside the radius of maximum wind at the level of maximum vortex strength.

To obtain the temperature perturbation, substitution is made for V_θ in (B3) and integration is performed inward from $r = R'$, where the temperature perturbation is assumed to be zero.

The Ertel PV can be written as

$$\text{PV} = \frac{1}{\rho}(\boldsymbol{\omega}\cdot\nabla\theta), \tag{B6}$$

where $\boldsymbol{\omega}$ is vector vorticity, θ is virtual potential temperature, and ρ is air density. To compute the potential vorticity in the center of the MCV, we continue to view the MCV as a wind and mass field perturbation superposed on a basic state of rest. The thermodynamics of the basic state is defined as that determined by linear interpolation of the three nearest 1200 UTC 9 June radiosonde observations [Denver (DEN), Dodge City

(DDC), North Platte (LBF)] to the approximate 2030 UTC position of the MCV center from Fig. 2. (Note the 0000 UTC 10 June soundings were not used because of strong influence by convection at Denver.) This interpolation is done by first identifying salient layers or levels present in the three raobs (e.g., top of nocturnal boundary layer, transition layer, previous day's mixed layer, tropopause, etc.) and then linearly interpolating observations at these levels to the MCV center position to estimate the pressure and potential temperature. The interpolated sounding was then modified to take into account daytime heating. The resulting basic-state sounding is the solid line shown in Fig. 16. The basic-state motion field is assumed to be at rest. This is warranted given Fig. 3.

With these definitions and assumptions, the potential vorticity at the center of the vortex can be written as

$$\mathrm{PV} = \left[\frac{RT_o}{P_o}e^{Z/H(\kappa+1)}\right]\left[f + \frac{2V_m(Z)}{r_m}\right] \cdot\left[\frac{\kappa}{H}(T' + T) + \frac{\partial T'}{\partial Z} + \frac{\partial T}{\partial Z}\right], \qquad \text{(B7)}$$

where T is the basic-state virtual temperature and T' is the modeled MCV perturbation virtual temperature, $g = 9.8\ \mathrm{m\ s^{-1}}$, $H = RT_o/g$, $\kappa = 2/7$, and other symbols have been defined previously. In order to avoid discontinuities in the depiction of potential vorticity, the virtual potential temperature of the basic-state sounding is represented as a natural cubic spline. In view of the assumptions used in the calculations (most notably, that of circularity of the vortex), these results are probably only valid to a factor of 2 or so in the size of the temperature and potential vorticity perturbations. In particular, if the vortex is in fact elongated in the east–west direction (section 5), the estimate of V_m may be too large and r_m too small. The effect would be to reduce the size of the temperature and potential vorticity perturbations.

REFERENCES

Augustine, J. A., and E. J. Zipser, 1987: The use of wind profilers in a mesoscale experiment. *Bull. Amer. Meteor. Soc.,* **68,** 4–17.

Bartels, D. L., and R. A. Maddox, 1991: Midlevel cyclonic vortices generated by mesoscale convective systems. *Mon. Wea. Rev.,* **119,** 104–118.

Brandes, E. A., 1990: Evolution and structure of the 6–7 May 1985 mesoscale convective system and associated vortex. *Mon. Wea. Rev.,* **118,** 109–127.

——, and C. L. Ziegler, 1993: Mesoscale downdraft influences on vertical vorticity in a mature mesoscale convective system. *Mon. Wea. Rev.,* **121,** 1337–1353.

Brown, J. M., K. R. Knupp, and F. Caracena, 1982: Destructive winds from shallow, high based cumulonimbi. Preprints, *12th Conf. on Severe Local Storms,* San Antonio, TX, Amer. Meteor. Soc., 272–275.

Bullock, C. S., J. S. Wakefield, J. M. Brundage, D. S. Walts, T. J. Le Febvre, P. A. Amstein, and L. B. Dunn, 1988: The DARE workstation and some lessons learned from its operational use. Preprints, *Fourth Conf. on Interactive Information and Processing Systems for Meteorology, Oceanography and Hydrology,* Anaheim, CA, Amer. Meteor. Soc., 70–76.

Charney, J. G., 1955: The use of primitive equations of motion in numerical prediction. *Tellus,* **7,** 22–26.

Chen, S. S., and W. M. Frank, 1993: A numerical study of the genesis of extratropical mesovortices. Part I: Evolution and dynamics. *J. Atmos. Sci.,* **50,** 2401–2426.

Cotton, W. R., L. Ming-Sen, C. J. Tremback, and R. L. McAnelly, 1989: A composite model of mesoscale convective complexes. *Mon. Wea. Rev.,* **117,** 765–783.

Cunning, J. B., 1986: The Oklahoma–Kansas preliminary regional experiment for STORM-Central. *Bull. Amer. Meteor. Soc.,* **67,** 1478–1486.

Davis, C. A., and M. L. Weisman, 1994: Balanced dynamics of mesoscale vortices produced in simulated convective systems. *J. Atmos. Sci.,* **51,** 2005–2030.

Fritsch, J. M., J. D. Murphy, and J. S. Kain, 1994: Warm-core vortex amplification over land. *J. Atmos. Sci.,* **51,** 1780–1807.

Fujita, T. T., 1959: Precipitation and cold air production in mesoscale thunderstorm systems. *J. Meteor.,* **16,** 454–466.

Hales, J. E., 1990: An examination of the development and role of a mesoscale vorticity center in the Council Bluffs tornado on 15 July 1988. Preprints, *16th Conf. on Severe Local Storms,* Kananaskis Park, AB, Canada, Amer. Meteor. Soc., 446–449.

Haynes, P. H., and M. E. McIntyre, 1987: On the evolution of vorticity and potential vorticity in the presence of diabatic heating and frictional or other forces. *J. Atmos. Sci.,* **44,** 828–841.

Houze, R. A., S. A. Rutledge, M. I. Biggerstaff, and B. F. Smull, 1989: Interpretation of Doppler weather radar displays of midlatitude mesoscale convective systems. *Bull. Amer. Meteor. Soc.,* **70,** 608–619.

Johnson, R. H., and D. L. Bartels, 1992: Circulations associated with a mature-to-decaying midlatitude mesoscale convective system. Part II: Upper-level features. *Mon. Wea. Rev.,* **120,** 1301–1320.

——, S. Chen, and J. J. Toth, 1989: Circulations associated with a mature-to-decaying midlatitude mesoscale convective system. Part I: Surface features—Heat bursts and mesolow development. *Mon. Wea. Rev.,* **117,** 942–959.

Johnston, E. C., 1981: Mesoscale vorticity centers induced by mesoscale convective complexes. M.S. thesis, Dept. of Meteorology, University of Wisconsin—Madison, 54 pp. [Available from University of Wisconsin—Madison, 1225 W. Dayton St., Madison, WI 53706-1695.]

Jorgensen, D. P., and B. F. Smull, 1993: Mesovortex circulations seen by airborne Doppler radar within a bow-echo mesoscale convective system. *Bull. Amer. Meteor. Soc.,* **74,** 2146–2157.

Leary, C. A., and E. N. Rappaport, 1987: The life cycle and internal structure of a mesoscale convective complex. *Mon. Wea. Rev.,* **115,** 1503–1527.

Lorenz, E. N., 1960: Energy and numerical weather prediction. *Tellus,* **115,** 364–373.

Maddox, R. A., 1980: Mesoscale convective complexes. *Bull. Amer. Meteor. Soc.,* **61,** 1374–1387.

——, 1983: Large scale meteorological conditions associated with midlatitude, mesoscale convective complexes. *Mon. Wea. Rev.,* **111,** 1475–1495.

McWilliams, J. C., 1988: Vortex generation through balanced adjustment. *J. Phys. Oceanogr.,* **18,** 1178–1192.

Menard, R. D., and J. M. Fritsch, 1989: A mesoscale convective complex-generated inertially stable warm core vortex. *Mon. Wea. Rev.,* **117,** 1237–1260.

Ooyama, K., 1982: Conceptual evolution of the theory and modeling of the tropical cyclone. *J. Meteor. Soc. Japan,* **60,** 369–380.

Phillips, N. A., 1973: Principles of large-scale numerical weather prediction. *Dynamical Meteorology,* P. Morel, Ed., Reidel, 1–96.

Raymond, J. D., and H. Jiang, 1990: A theory for long-lived mesoscale convective systems. *J. Atmos. Sci.,* **47,** 3067–3077.

Skamarock, W. C., M. L. Weisman, and J. B. Klemp, 1994: Three-

dimensional evolution of simulated long-lived squall lines. *J. Atmos. Sci.,* **51,** 2563–2584.

Smull, B. F., and R. A. Houze Jr., 1985: A midlatitude squall line with a trailing region of stratiform rain: Radar and satellite observations. *Mon. Wea. Rev.,* **113,** 117–133.

Stensrud, D. J., R. A. Maddox, and C. L. Ziegler, 1991: A sublimation-initiated mesoscale downdraft and its relation to the wind field below a precipitating anvil cloud. *Mon. Wea. Rev.,* **119,** 2124–2139.

Strauch, R. G., D. A. Merritt, K. P. Moran, K. B. Earnshaw, and D. van de Kamp, 1984: The Colorado wind-profiling network. *J. Atmos. Oceanic Technol.,* **1,** 97–109.

van de Kamp, D. W., 1988: Principles of wind profiler operation. Wind Profiler Training Manual 1, 49 pp. [Available from Environmental Research Laboratories, Boulder, CO 80303.]

Velasco, I., and J. M. Fritsch, 1987: Mesoscale convective complexes in the Americas. *J. Geophys. Res.,* **92,** 9591–9613.

Wang, W., Y. H. Kuo, and T. T. Warner, 1993: A diabatically driven mesoscale vortex in the lee of the Tibetan Plateau. *Mon. Wea. Rev.,* **121,** 2542–2561.

Weber, B. L., D. B. Wuertz, D. C. Law, A. S. Frisch, and J. M. Brown, 1992: Effects of small-scale vertical motion on radar measurements of wind and temperature profiles. *J. Atmos. Oceanic Technol.,* **9,** 193–209.

Zhang, D. L., and J. M. Fritsch, 1986: Numerical simulation of the meso-β scale structure and evolution of the 1977 Johnstown flood. Part I: Model description and verification. *J. Atmos. Sci.,* **43,** 1913–1943.

——, and ——, 1987: Numerical simulation of the meso-β scale structure and evolution of the 1977 Johnstown flood. Part II: Inertially stable warm-core vortex and the mesoscale convective complex. *J. Atmos. Sci.,* **44,** 2593–2612.

——, and ——, 1988a: Numerical sensitivity experiments of varying model physics on structure, evolution and dynamics of two mesoscale convective systems. *J. Atmos. Sci.,* **45,** 261–293.

——, and ——, 1988b: A numerical investigation of a convectively generated, inertially stable, extratropical warm-core mesovortex over land. Part I: Structure and evolution. *Mon. Wea. Rev.,* **116,** 2660–2687.